Efficient Second-Harmonic Generation in Si-GaP Asymmetric Coupled-Quantum-Well Waveguides

Efficient Second-Harmonic Generation in Si-GaP Asymmetric Coupled-Quantum-Well Waveguides

Francesco De Leonardis, Richard Soref, *Life Fellow, IEEE,*

***Abstract*—We present a theoretical investigation of efficient second harmonic generation in the cubic lattice-matched N-doped Si/GsP multiple quantum well system integrated in a strip waveguide in the silicon-on-insulator platform. A "giant" second-order nonlinear optical susceptibility is obtained in an asymmetric coupled quantum well (ACQW) stack by engineering the 1-2 and 1-3 inter-subband spacings for resonance at both a ~4 μm pump wavelength and a ~2μm harmonic wavelength. Generation has been simulated as a function of the quantum well physical parameters, the infrared absorption losses, and the detuning from the double resonance condition. For TM pumps at 3.75 μm and 4.24 μm, a $\chi_{zzz}^{(2)}$ value ranging from 7.73×10^3 pm/V to 1.13×10^4 pm/V has been calculated and a maximum conversion efficiency ranging between 1.23 %/W and 1.68%/W has been obtained, where the waveguide coherence length was 5.57 μm and 6.16 μm.**

***Index Terms*—Optical waveguides; Nonlinear optical devices; Second Harmonic Generation; Quantum Well, SOI Technology.**

I. Introduction

Nonlinear optical effects comprise an important area of current research in Group-IV photonic and optoelectronic circuits. For manufacturing opto-electronic integrated circuits (OEICs) and photonic integrated circuits (PICs) upon both silicon-on-insulator (SOI) and silicon on nitride (SON) substrates, the monolithic technological approach is preferred over hybrid solutions. However, the second-order term of the nonlinear susceptibility tensor cannot be exploited in diamond-cubic metal–oxide–semiconductor (CMOS)-compatible materials (for example, Si, Ge and SiGeSn) because $\chi^{(2)}$ vanishes in the dipole approximation [1]. This provides a significant challenge for second-order nonlinear processes such as second-harmonic generation (SHG) and phase-only modulation in a CMOS-compatible platform. For these reasons, the third- or higher-order nonlinearities of Si [2] have been adopted in order to enable functions such as amplification and lasing, wavelength conversion and optical processing [3]. However, third-order nonlinearities require relatively high optical powers, and can compete with nonlinear-loss mechanisms such as two-photon absorption and two-photon induced free-carrier absorption. Thus it would be desirable to create $\chi^{(2)}$ in silicon-based Group-IV photonic circuits in order to enable a new array of CMOS-compatible optical devices capable of nonlinear functionalities such as Pockels electro-optic modulation, second harmonic generation (SHG), sum frequency up-conversion, and difference frequency generation. Therefore, the key to induce $\chi^{(2)}$in centrosymmetric crystals such as Si and Ge is to break the symmetry. In this context, several works have demonstrated that $\chi^{(2)}$ could be induced by breaking the symmetry via induced mechanical stress and strain [4]-[6]. Second-Harmonic-Generation (SHG) experiments and first-principle calculations have been carried out at optical wavelengths in a Si waveguide by using a stressing silicon-nitride overlayer [7]-[8]. An asymmetry can also be introduced into the crystalline structure of a material in the presence of an applied DC electric field, because the dipole moments orient themselves in the direction of the applied field. As a result, the SHG process is realized via the third-order nonlinear susceptibility. This electric-field-induced SHG (EFISHG) has been demonstrated in integrated silicon ridge waveguides via compact p-i-n junctions [9]. Besides these approaches, the symmetry breaking can be artificially realized with a pair of doped asymmetric coupled quantum wells (ACQWs), in which three of the quantum-confined states are equidistant in energy, resulting in a double resonance for pump and SHG. The giant nonlinearity of intersubband transitions is observed as a result of the giant dipole moment of a two-dimensional (2D) carrier gas in a doped quantum well. Although the giant nonlinearity ACQWs was investigated more than two decades ago, both theoretically [10] and experimentally [11,12], it has been revisited in recent studies involving n-doped InGaAs/AlInAs quantum wells on InP substrates [13-15]. The band offset of 0.5

Manuscript received xxx x, 2021; revised xxx x, xxxx.

Richard A. Soref is with the University of Massachusetts at Boston.

F. De Leonardis, is with the Photonics Research Group, Department of Electrical and Information Engineering, Politecnico di Bari, Via Orabona 4, Bari, 70126, Italy. (e-mail: francesco.deleonardis@poliba.it).

eV makes this platform suitable for nonlinear photonics operating in the Mid-Infrared Region (MIR). However, compound semiconductor heterostructures are not ideal for mass-production based on the CMOS foundry. To overcome this drawback, giant $\chi^{(2)}$ has been recently demonstrated in p-doped SiGe/Si ACQW [16,17], opening the possibility of improving the performance of second-order nonlinear devices in OEICs and PICs based on the Group-IV platform, such as MIR emission sensors based on second-harmonic generation (SHG). However, the ACQWs based on SiGe/Si platform are limited to operation with a pump wavelength ranging between 9.6 μm and 10 μm [16,17], inhibiting the generation of the second harmonic signal in the wavelength range of telecom interest [18]. To enable harmonic generation in telecom-related, fiber-related platforms, we theoretically investigate the possibility of inducing SHG around 2 μm [18] in ACQW structures realized on SOI or SON wafers. In order to realize foundry manufacture of our structure, the wafer would be partially processed in the foundry, including local removal of Si strip regions to reveal the SiO_2 or Si_3N_4 top surface for subsequent MBE multi-layer depositions. Those local-area MB epitaxies would be performed outside of the foundry, and after that the wafer would be returned to the foundry to complete the processing. In particular, our aim is to demonstrate the feasibility of an integrated waveguide in order to perform SHG with high conversion efficiency. For this aim, we propose the new lattice-matched heterostructure, the (111) Si/GaP ACQW system, for which we report a study of intersubband properties relevant to the $\chi^{(2)}$ susceptibility.

The paper is organized as follows. The theoretical background for the SHG effect in an SOI MQW optical waveguide based on ACQW structures is reported in Section 2. The theoretical calculations for the $\chi^{(2)}$ susceptibility and SHG process are reported in Section 3. In particular, theoretical investigations of the conversion efficiency are presented as a function of ACQW parameters, absorption losses, and detuning from the double resonance conditions. Finally, Section 4 summarizes the conclusions.

II. Theoretical Background

In this section we describe the Second Harmonic Generation (SHG) process induced by the giant $\chi^{(2)}$ susceptibility generated in heterostructures such as the (111) Si/GaP asymmetric coupled quantum well (ACQW) system. The tight-binding (TB) parameters for both bulk Si and GaP are taken from the article by Vogl, Hjalmarsson, and Dow [19]. A key parameter for the heterostructure is the band offset. Recently, a valence-band (VB) offset of 0.24 eV was measured in [20]. With the values listed in [19], this translates into a conduction-band (CB) offset of 0.98 eV. We are aware that the value measured in [20] refers to a growth condition different than that assumed here. However, in the absence of measurements matched to our growth condition, we assume 0.24 eV as a starting point to demonstrate the feasibility of obtaining giant $\chi^{(2)}$ in (111) Si/GaP ACQWs. Additionally, the VB offset can be considered here as a fitting parameter to be set together with a relaxation time τ_Γ for all intersubband transitions, in order to match our model to future experimental $\chi^{(2)}$ measurements.

The first question we address is the role of the various valleys in generating confined states. Si has the X (more exactly Δ) state as the conduction minimum with the Γ_{15c} state lower in energy than the Γ_{1c} state. In this context, Si is the quantum well for holes, X electrons, and Γ_{15c} electrons, while GaP is the well for Γ_{1c} electrons. Due to the small valence-band offset, we calculate $\chi^{(2)}$ considering CB intersubband transitions, where the double resonance condition can be achieved. Indeed, the design criterion for SHG in ACQWs is that the intersubband transition energies $\hbar\omega_{12} = (E_2 - E_1)$ and $\hbar\omega_{23} = (E_3 - E_2)$ (where E_i is the confined energy of the i-th subband) should both be in resonance with the pump photon energy $\hbar\omega_{p0} = \hbar\omega_{12} = \hbar\omega_{23}$. The second question we address is the optimal choice for the direction growth. In silicon the three doubly degenerate X valleys, hereafter indicated as X_1, X_2 and X_3, are oriented along the direction [1 0 0], [0 1 0] and [0 0 1], respectively. Hereafter, we set the z axis parallel to the carrier confinement direction (i.e. orthogonal to the QW growth plane). Under the generalized effective mass tensor scenario and for the (0 0 1) Si wafer, the effective mass tensor element, m^*_{zz}, corresponds to m^*_t(transverse effective mass) and m^*_l(longitudinal effective mass) for X_1, and X_2, X_3, respectively. To the contrary, (1 1 1) Si/GaP guarantees $m^*_{zz} = 3m^*_l m^*_t/(m^*_t + 2m^*_l)$ for all X valleys. Thus, for the [1 1 1] growth direction, the x axis and the y axis were chosen along [$\bar{2}$ 1 1]and [0 $\bar{1}$ 1] directions, respectively. The anisotropic effects in a multivalley semiconductor can be taken into account by writing the energy-momentum dispersion function in the general form with effective mass tensor: $\varepsilon(\boldsymbol{k}) = \sum_{i,j} k_i k_k / m^*_{ij}$ $(i, j = x, y, z)$. Even though the transverse and perpendicular motions are separated in eigenvalues and eigenfunction in the one-band approximation, the two motions are still coupled in the intersubband optical transitions. It can be shown that the optical transition matrix element in the quantum well can be written in the dipole approximation as [21]:

$$\left|\langle\psi_n|r_j|\psi_m\rangle\right| = \frac{\hbar^2}{(E_n - E_m)}\left(\frac{1}{m^*_{zr_j}}\right)\left|\langle F_n|\nabla_z|F_m\rangle\right| \quad (1)$$

where ψ_i and F_i are the subband wavefunction and the envelope function, respectively. The terms r_j stands for x, y, z when $j = 1,2,3$. It is worth to noting that when the one-band approximation is not appropriate, Eq. (1) becomes more complicated and requires higher-order terms to describe the coupling between Bloch functions. For our purpose here, we think that the treatment of the dominant band is satisfactory.

In this context, the second-order susceptibility tensor for the case of second-harmonic generation near double resonance is given by [10,21,22]:

$$\chi^{(2)}_{ijk} = \frac{e^3}{\varepsilon_0}(N_1 + 2N_2 - N_3)\frac{\left|\langle\psi_1|r_i|\psi_3\rangle\right|\left|\langle\psi_3|r_j|\psi_2\rangle\right|\left|\langle\psi_2|r_k|\psi_1\rangle\right|}{(\hbar\omega_{12} - \hbar\omega_p + j\hbar\Gamma)(\hbar\omega_{31} - 2\hbar\omega_p + j\hbar\Gamma)} \quad (2)$$

where N_i is the three-dimensional intensity-dependent density, populating subband i-th and satisfying the relationship $N_1 + N_2 + N_3 = N$, where N is the overall three-dimensional electron density averaged over the ACQW period. The term $\Gamma = 1/\tau_\Gamma$ defines the linewidth of the $\chi^{(2)}_{ijk}$ spectrum. Since τ_Γ is not available in the literature for the materials used in this work, we have assumed τ_Γ=0.1ps, according to the values generally adopted in literature for several platforms. Additionally, experimental measurements of linewidth of the $\chi^{(2)}_{ijk}$ spectrum could be used to better set the values of τ_Γ in order to improve the model predictions of the SHG efficiency.

Equations (1) and (2) indicates that the in-plane (x, y) transition matrix elements are non-negligible as long as the effective-mass tensor is anisotropic and has nonzero off-diagonal components, as in the case considered here ([1 1 1] growth direction). Moreover while $\chi^{(2)}_{zzz}$ is the same for all the X valleys, we observe that $\chi^{(2)}_{xzx}$ assumes two different values for X_1, and X_2, X_3, respectively, as a result of $m^{*(X_1)}_{zx} \neq m^{*(X_2)}_{zx} = m^{*(X_3)}_{zx}$. However, hereafter, we evaluate the SHG process induced by $\chi^{(2)}_{zzz}$, for which the TM polarization is required for both pump and SH waves.

According to the nonlinear coupled mode theory (CMT) [23], the equations describing the power transfer between the pump (p) and the second harmonic (SH) waves can be written as (3)-(4). In particular, a_1 and a_2 represent the slowly varying field amplitudes (y functions, with y the propagation direction.) for the pump and second harmonic TM modes. The term $\Delta k = 4\pi n_{eff,p}/\lambda_p - 2\pi n_{eff,SH}/\lambda_{SH}$ is the mismatch between the pump and second harmonic propagation constants, with $n_{eff,p}$, and $n_{eff,SH}$ the effective refractive index for pump and SH optical modes, respectively. Moreover, the coefficient f_{112} represents the overlap integral of pump and second harmonic fundamental TM modes, defined as in [23].

$$\frac{da_1}{dy} = -\frac{1}{2}\Gamma_p(\alpha_{12} + \alpha_{23})a_1 + j2f_{112}\frac{\omega_p \varepsilon_0 c_0^{3/2}\mu_0^{3/2}\chi^{(2)}_{zzz}}{\sqrt{2n^2_{eff,p}\cdot n_{eff,SH}}}a_2 a_1^* e^{j\Delta k y} \quad (3)$$

$$\frac{da_2}{dy} = -\frac{1}{2}\Gamma_{SH}(\alpha_{13})a_2 + jf_{112}\frac{\omega_{SH}\varepsilon_0 c_0^{3/2}\mu_0^{3/2}\chi^{(2)}_{zzz}}{\sqrt{2n^2_{eff,p}\cdot n_{eff,SH}}}a_1 a_1 e^{-j\Delta k y} \quad (4)$$

where c_0, Γ_p and Γ_{SH} are the light velocity and the confinement factor for the pump and SH optical modes inside the active region, respectively. As shown by Eqs. (3)-(4), in a ACQW system, intersubband absorption of both the pump and second-harmonic waves occurs in parallel with the second-harmonic generation. The absorption coefficient α_{ij} $(ij = 1,2,3)$ are given by [24]:

$$\alpha_{ij}(\omega) = \frac{e^2\hbar\omega(N_i - N_j)\left|\langle\psi_i|z|\psi_j\rangle\right|^2\hbar\Gamma}{\varepsilon_0\cdot\hbar\cdot c_0\cdot n(\omega)\left[\left(\hbar\omega - E_{ij}\right)^2 + (\hbar\Gamma)^2\right]} \quad (5)$$

III. Numerical Results

An efficient SHG process can be achieved in integrated waveguides if a large number (N_p) of ACQW periods is grown stacked within a strip to fill the required strip height, resulting in a maximization of the overlap between the active region and the optical modes. Although both SOI and SON platforms are suitable to realize the SHG process originated by the giant $\chi^{(2)}$ induced in the ACQW system, we focus our investigation mainly on SOI. In this context, a fully-etched waveguide cross-sections with a width *W* and height *H*, is considered and sketched in Fig. 1, where a cover of SiO_2 is assumed.

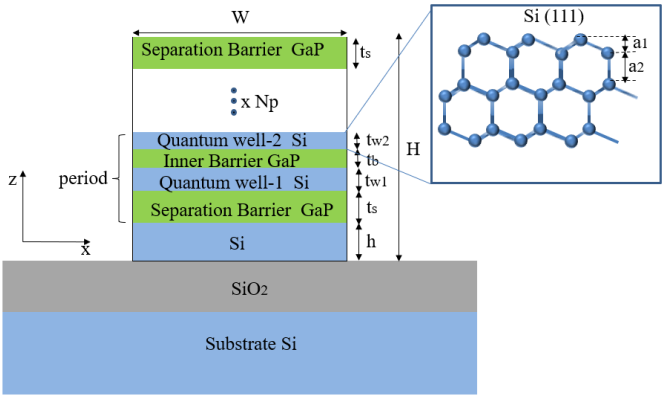

Fig. 1. Si-GaP ACQW waveguide cross section based on the SOI platform. Inset: Interplanar spacing for silicon in the [1 1 1] direction.

Note that while the interplanar spacing of Si (100) and Si (110) are 1.36 Å and 1.92 Å, respectively, the crystal plane (111) is the cleavage plane of silicon, which has short interplanar spacing (a_1=0.78 Å) and long interplanar spacing (a_2=2.35 Å) [25] (see inset of Fig. 1). In the lack of experimental data on the epitaxial growth of Si on GaP along the direction [1 1 1], we can assume two different sequences: a_1-a_2---a_2-a_1 and a_2-a_1----a_1-a_2. As a result, with five interplanar spacings, quantum well thickness of 0.7 nm and 0.86 nm can be realized, respectively.

With the aim of theoretically demonstrating the feasibility of efficiently generating the second harmonic wave, numerical simulations for both optical and electronic parts have been performed by using a finite element method (FEM to determine the physical parameters for evaluating Eqs. (1)-(5). In particular, due to the increasing interest recently demonstrated in fiber-optical telecommunications links working around 2 μm [18], hereafter we will design the ACQW structures to be doubly resonant for a pump wavelength around 4 μm.

The plot in Fig. 2 shows the transitions energies $E_{12} = (E_2 - E_1)$ and $E_{23} = (E_3 - E_2)$ as a function of the quantum well-1 thickness for t_{w2} of 0.7 nm and 0.86 nm, assuming the inner barrier thickness t_b=1 nm. The control of layer thickness down to 0.7 nm, would be done by modern Molecular Beam Epitaxy (MBE) as evidenced by the experimental results in [26]. The curves indicate that the double resonance condition is achieved at $\hbar\omega_{p0} \cong$ 0.331 eV ($\lambda_{p0} \cong$3.752 μm) and 0.292 eV ($\lambda_{p0} \cong$ 4.241 μm) for t_{w1}= 1.51 nm, t_{w2}= 0.7 nm and for t_{w1}= 1.8 nm, t_{w2}= 0.86 nm, respectively. Thus hereafter, we will

consider two different structures, named ACQW-1 and ACQW-2, having the following sets of thickness: t_b=1 nm, t_{w1}= 1.51 nm, t_{w2}= 0.7 nm, t_s=10.5 nm and t_b=1 nm, t_{w1}= 1.8 nm, t_{w2}= 0.86 nm, t_s=8 nm, respectively. For our two structures, the QW layer thicknesses are extremely thin, comprising just a few atomic monolayers. That is why our Si/GaP QW structures are "beginning to resemble" a Si/GaP short-period superlattice, which is also an excellent candidate for offering giant $\chi^{(2)}$.

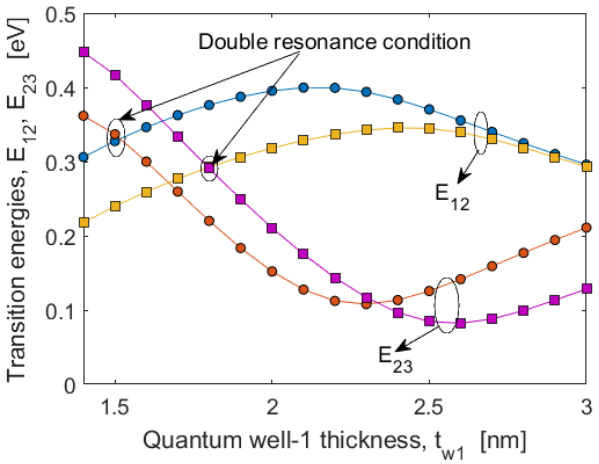

Fig. 2. Transition energies for Si-GaP ACQW structure. Circle: t_{w2}= 0.7 nm and t_b=1 nm; Squares: t_{w2}= 0.86 nm and t_b=1 nm.

Some comments about the waveguide cross-section are worth making. Since the selected pump wavelength is in the Mid-IR region where the SiO_2 induces absorption, W and H should be chosen in order to reduce the field tails inside the SiO_2 and then maximize the confinement factor into the strip region. Our preliminary FEM simulations indicated that a good trade-off is obtained with W=2 μm, and H=2.068 μm (2.34 μm), (by setting N_p=150 (200) and h=100 nm, t_s=10.5 nm (8 nm)), for the ACQW-1 (ACQW-2) structure. The calculated confinement factors into the strip are Γ_p=0.94 and Γ_{SH}=0.99 for both ACQW-1 and ACQW-2 systems. Under this condition, the absorption induced by SiO_2 is made strongly negligible with respect to the absorption losses induced by α_{ij} (see Eq. (5)). We think that the ACQW-based waveguides can be end-fire coupled to SOI strips by depositing the MQW locally in a "trench" that is etched in the strip-photonic "circuit". Moreover, in the case of "mid infrared" waveguides of Si_3N_4 upon SiO_2, an evanescent-wave side-coupling from Si_3N_4 into/out-of the ACQW grown upon the Si_3N_4 strip's top surface could be adopted.

At this point, we address the calculation of the $\chi^{(2)}_{ijk}$ susceptibility, according to Eq. (2). Generally in the ACQW systems, the sheet density per period (N_s) is employed in order to determine the 3-D electron density N. Hereafter we assume for all simulations N_s=5×10^{11} cm^{-2}. It is worth outlining that the intensity-dependent electron density is governed by the rate equations given in [24], where the time evolution of N_i is influenced by the density of photons at ω_p and $2\omega_p$, absorbed from the ACQW structure. In this context, we have numerically solved the above-mentioned rate equations coupled with Eqs.(2)-(5). The results, not shown here for compactness reasons, indicate that for input pump power typically employed in the integrated waveguide, the N_i values are very close to the subband population at the thermal equilibrium: N_1=3.6454×10^{17} (4.2881×10^{17}) cm^{-3}, N_2=1.0166×10^{12} (5.2298×10^{12}) cm^{-3}, and N_3=2.6747×10^6 (6.8411×10^7) cm^{-3}, for the system ACQW-1 (ACQW-2).

TABLE I
PHYSICAL PARAMETERS FOR N_s=5×10^{11} cm^{-2} AND τ_Γ=0.1 ps

Parameters	ACQW-1 λ_{p0}=3.752 μm	ACQW-2 λ_{p0}=4.241 μm
$\langle\psi_2\|z\|\psi_1\rangle$ (nm)	0.30	0.29
$\langle\psi_3\|z\|\psi_2\rangle$ (nm)	0.50	0.51
$\langle\psi_1\|z\|\psi_3\rangle$ (nm)	0.35	0.44
$\langle\psi_2\|x\|\psi_1\rangle$ X_1 (nm)	0.16	0.15
$\langle\psi_3\|x\|\psi_2\rangle$ X_1 (nm)	0.26	0.26
$\langle\psi_2\|x\|\psi_1\rangle$ X_2, X_3 (nm)	0.077	0.076
$\langle\psi_3\|x\|\psi_2\rangle$ X_2, X_3 (nm)	0.13	0.13
Peak $\chi^{(2)}_{zzz}$ (pm/V)	7.73×10^3	1.13×10^4
Peak $\chi^{(2)}_{zxx}$ X_1(pm/V)	2.08×10^3	3.05×10^3
Peak $\chi^{(2)}_{zxx}$ X_2, X_3 (pm/V)	522	762.73
$n_{eff,p}$	2.8868	2.8866
$n_{eff,SH}$	3.0583	3.0573
Coherence length, $L_c = \pi/\Delta k$ (μm)	5.47	6.21

Table I provides the calculated physical parameter values which demonstrate giant $\chi^{(2)}_{ijk}$ values, ranging between 522 pm/V and 7.73×10^3 pm/V and between 762.73 pm/V and 1.13×10^4 pm/V for ACQW-1 and ACQW-2, respectively. Moreover, the large calculated off-diagonal tensor components $\chi^{(2)}_{zxx}$ thus open interesting opportunities to realize TE-TM polarization mixing in nonlinear phenomena.

Note that the short coherence length (L_c), obtained here, is in good agreement with the values of 5.08 μm [9], for SHG in integrated strained silicon waveguides. However, the coherence length can be modified by acting on the detuning values $\hbar\omega_p$-$\hbar\omega_{12}$ and $2\hbar\omega_p$- $\hbar\omega_{13}$, which, in turn, induces change in $\Delta n_{abs}(\omega_p)$ and $\Delta n_{abs}(2\omega_p)$. These terms represent the refractive index change induced by photon absorptions (see Eq. (5)) via the Kramers-Kronig relation [24], and they have been included in the ACQW layer's bulks refractive index in our FEM simulations. In particular, if the signs of the detunings are chosen both positive, the overall negative contributions of $\Delta n_{abs}(\omega_p)$ and $\Delta n_{abs}(2\omega_p)$, with $|\Delta n_{abs}(2\omega_p)| > |\Delta n_{abs}(\omega_p)|$, partially compensates the phase mismatching, resulting in an increasing of the coherence length. The opposite trend is recorded for detunings both negative. As an example, $\Delta n_{abs}(\omega_p)$ and $\Delta n_{abs}(2\omega_p)$ is evaluated in -0.0065 (-0.0051) and -0.0103 (-0.019) for λ_p=3.7 μm (4.2 μm), for the system ACQW-1 (ACQW-2). Moreover, while $\chi^{(2)}_{ijk}$ is largest at the double resonance condition, the maximum SHG efficiency takes place for a detuning condition that guarantees the trade-off between reduced absorption losses and diminished nonlinear susceptibility. All these effects are observable in Figs. 3 (a) and (b), where the color map for the second harmonic generation efficiency, $\eta = P_{SH}(L)/P^2_{p,in}$, ($P_{p,in}$ is the input pump power) is plotted in the plane waveguide length and (L)-

This article has been accepted for publication in IEEE/OSA Journal of Lightwave Technology. This is the author's version which has not been fully edited and content may change prior to final publication. Citation information: DOI 10.1109/JLT.2022.3143169

pump wavelength, for ACQW-1 and ACQW-2, respectively.

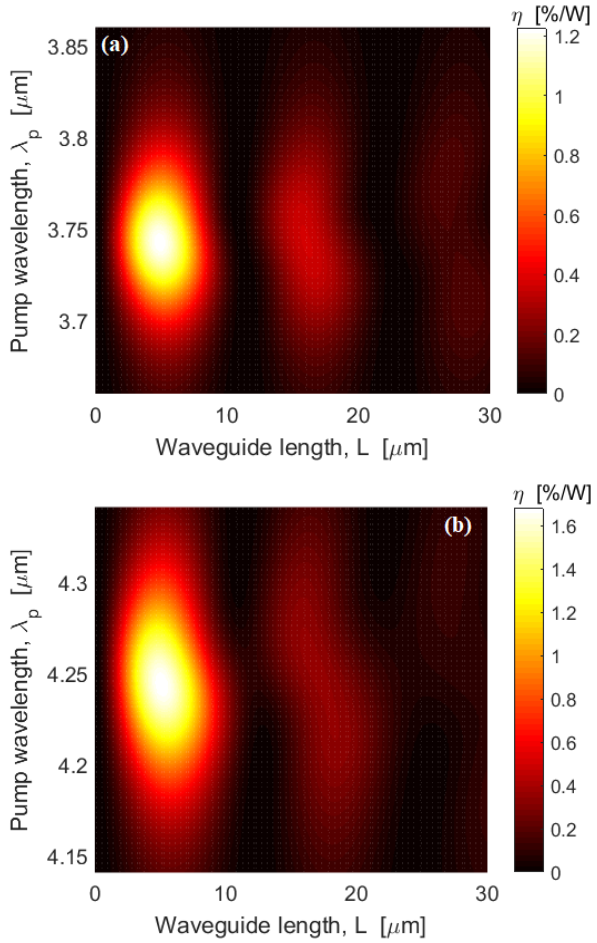

Fig. 3. Color map for the SHG efficiency in the plane L -λ_p: (a) ACQW-1 based waveguide; (b) ACQW-2 based waveguide

Although an oscillating profile versus the waveguide length is expected, the strong pump depletion, induced by the absorption losses (α_{ij}), makes the secondary efficiency peaks attenuated (see Fig. 3). Indeed, we calculated that the pump absorption length ranges from 22.66 μm (22.64 μm) to 22.38 μm (22.61 μm), when changing λ_p from 3.743 μm (4.244 μm) to 3.752 μm (4.241 μm), for the ACQW-1 (ACQW-2) structure. In the same operative condition, we recorded that the coherence length changes from 5.57 μm and 6.16 μm to 5.47 μm and 6.21 μm, for ACQW-1 and ACQW-2, respectively. These values ensure that the SHG process is strongly spatially localized in the waveguide. Indeed, we find η_{max} of 1.23%/W (at λ_p=3.743 μm, L=4.87 μm) and 1.68%/W (at λ_p=4.244 μm, L=5.11 μm) for ACQW-1 and ACQW-2, respectively. The plots of Fig. 3, therefore, demonstrate that few-micrometer length waveguides can be used to up-convert pump wave around 4 μm of wavelength to their second-harmonic with efficiencies up to 1.68%/W. Note that the waveguide lengths found here are comparable with the values of 3.7 μm and 7.6 μm, used in order to obtain the highest third-harmonic generation conversion efficiency reported to date in a silicon-based structure [27].

The performances of the SHG process in integrated waveguides, considered here are compared with those of alternative literature-cited platforms, in terms of the $\chi^{(2)}_{ijk}$ value and SHG efficiency. The results are summarized in Table II. As above mentioned, the linewidth of $\chi^{(2)}_{zzz}$ is strongly dependent on the relaxion time τ_Γ, which, in turn, is influenced by the scattering at the heterointerfaces. As a result, τ_Γ less than 0.1 ps (assumed in the simulations) could be recorded in the experiments. Thus, a reduction of τ_Γ induces both an increasing of the $\chi^{(2)}_{zzz}$ linewidth and a decreasing of the SHG efficiency. Our simulations indicate that the SHG efficiency changes quadratically with τ_Γ according to $\eta = a\tau_\Gamma^2 + b\tau_\Gamma + c$, where η is expressed in %/W and τ_Γ in ps. For ACQW-2 we have: a=7.4x10^2, b=-89 and c=3, resulting in an efficiency change from 1.68%W to 0.15%/W for τ_Γ of 0.1 ps and 0.05 ps, respectively. Although a heavy efficiency drop is recorded, the obtained value is still comparable with the other platforms (see Table II).

At this point, we analyze of the effects of the tolerance of fabrication on the SHG efficiency is carried on, by considering a change Δt_{w1} (deviation or error in the QW thickness) with respect to the t_{w1} values, designed to satisfy the double resonance condition.

TABLE II
COMPARISON BETWEEN DIFFERENT PLATFORM

Platform	Type	$\chi^{(2)}_{ijk}$ (pm/V)	η %/W	Ref.
Si	strained	40	7.9×10^{-6}	7
Si	EFISHG QPM	41	0.9-12	9
SiN	resonant	0.04	0.1	28
GaN	resonant	16	0.02	29
Si/GaP	ACQW-1 on SOI	1.585×10^4	1.23	This work
Si/GaP	ACQW-2 on SOI	2.051×10^4	1.68	This work
Si/GaP	ACQW-1 on SON	1.572×10^4	1.22	This work
Si/GaP	ACQW-2 on SON	2.028×10^4	1.66	This work

The results of the investigations are summarized in Fig. 4, where $\lambda_p = \lambda_{p0}$ (double resonance condition), and L=4.87μm and L=5.11 μm, have been assumed for ACQW-1 and ACQW-2 structures, respectively. We record that the efficiency is sensitive to layer errors and drops to the value of 0.1%/W when Δt_{w1} reaches +0.1 nm, depending mainly on the fact that we operate in an off-resonance condition and far from the maximum generated SH power obtained for waveguide length different from L=4.87 μm or L=5.11 μm.

Finally, some comments about the TB method are worth making. In order to improve the accuracy of the semiempirical TB method, in recent years, TB has been greatly improved by the introduction of several ab-initio TB methods. The resulting ab-initio TB models are compatible with the typical TB form and reproduce the selected ab-initio energy bands with high accuracy [30]. However, these projection-based methods have their own challenges. First, the corresponding time-consuming ab-initio calculations must be performed before the TB Hamiltonian construction, which hinders massive high-

throughput investigations [30]. This is particularly true in our case where the aim is to demonstrate the feasibility of giant $\chi^{(2)}_{zzz}$ in (111) Si/GaP ACQWs. To overcome the time-consumption drawback, the TB Hamiltonian parameterization based on machine learning techniques has been proposed very recently in [30]. However, we think that semiempirical TB method adopted here is sufficient, especially in view of the lack-of-knowledge of the (111) Si/GaP platform.

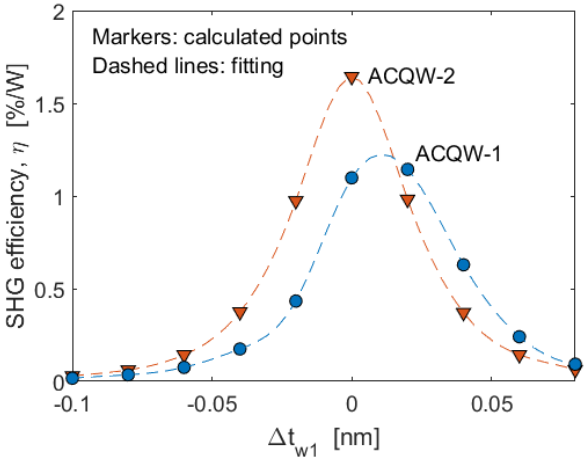

Fig. 4. SHG efficiency versus Δt_{w1} for both ACQW-1 and ACQW-2 based waveguides, operating at $\lambda_p = \lambda_{p0}$.

IV. Conclusion

In this paper, a detailed engineering procedure has been performed in order to optimize the SHG process in an integrated waveguide based on asymmetric coupled quantum well structures. We have explored the giant nonlinearity effect in N-doped lattice-matched Si/GaP asymmetric coupled quantum wells on the SOI (SON) substrate. Due to the relative large 0.98 eV electron band offset, the proposed structures can induce the double resonance condition for pump photon energy between 0.331 eV and 0.292 eV, extending the field of applications for the ACQW-induced second order nonlinearity beyond the range observed for III-V and $Si_{1-x}Ge_x$ heterostructures. The first estimation for diagonal and off-diagonal tensor components of $\chi^{(2)}_{ijk}$ has been presented here. In particular, two different asymmetric coupled quantum wells, satisfying the double resonance condition for second harmonic generation at 2 μm, have been designed with the aim of meeting the increasing interest for fiber-optical telecommunications links. In this context, general physical features have been investigated by means of a comparative analysis of the SH generation performance as a function of the quantum well physical parameters, the infrared absorption losses, and the detuning from the double resonance condition. Finally, we have demonstrated that few-micrometer length waveguides can be used to up-convert the pump wave to its second-harmonic with efficiency ranging between 1.23 %/W and 1.68%/W, due to the giant $\chi^{(2)}_{zzz}$ value ranging from 7.73×10^3 to 1.13×10^4.

Acknowledgment

R. S. Author is supported by the Air Force Office of Scientific Research on grant FA9550-21-1-0347.

References

[1] R. W. Boyd, "Nonlinear Optics", 2nd Edn, Academic, 2002.
[2] Q. Lin, O. J Painter, G. P. Agrawal, "Nonlinear optical phenomena in silicon waveguides: Modeling and applications," Opt. Express, 25, 16604-16644 (2007).
[3] J. Leuthold, C. Koos, W. Freude, "Nonlinear silicon photonics," Nature Photon. 4, 535-544 (2010).
[4] Z. Chen, J. Zhao, Y. Zhang, G. Jia, X. Liu, C. Ren, W. Wu, J. Sun, K. Cao, S. Wang., and B. Shi, "Pockel's effect and optical rectification in (111)-cut near-intrinsic silicon crystals," Appl. Phys. Lett. 92, 251111 (2008).
[5] S. V. Govorkov, V. I. Emel'yanov, N. I. Koroteev, G. I. Petrov, I. L. Shumay, V. V. Yakovlev, and R. V. Khokhlov, "Inhomogeneous deformation of silicon surface layers probed by second-harmonic generation in reflection," J. Opt. Soc. Am. B 6(6), 1117-1124 (1989).
[6] J.-H. Zhao, Q.-D. Chen, Z.-G. Chen, G. Jia, W. Su, Y. Jiang, Z.-X. Yan. T. V. Dolgova, O. A. Aktsipetrov, H.-B. Sun, "Enhancement of second-harmonic generation from silicon stripes under external cylindrical stain," Opt. Lett. 34(21), 3340–3342 (2009).
[7] M. Cazzanelli, F. Bianco, E. Borga, G. Pucker, M. Ghulinyan, E. Degoli, E. Luppi, V. Véniard, S. Ossicini, D. Modotto, S.Wabnitz, R. Pierobon, and L. Pavesi "Second-harmonic generation in silicon waveguides strained by silicon nitride," Nature Mater. 11(2), 148–154 (2011).
[8] N. K. Hon, K. K. Tsia, D. R. Solli, and B. Jalali, "Periodically poled silicon," Appl. Phys. Lett. 94, 091116 (2009).
[9] E. Timurdogan, C. V. Poulton, M. J. Byrd, M. R. Watts, "Electric field-induced second order nonlinear optical effects in silicon waveguides," Nature Photonics, 11, 200-206 (2017).
[10] E. Rosencher, Ph. Bois, "Model system for optical nonlinearities: Asymmetric quantum wells," Physical Review B,44(20), 11315-11327 (1991).
[11] E. Rosencher, A. Fiore, B. Vinter, V. Berger, Ph. Bois, and J. Nagle, "Quantum Engineering of Optical Nonlinearities," Science, 271(5246), 168-173 (1996).
[12] K. L. Vodopyanov, K. O'Neill, G. B. Serapiglia, C. C. Phillips, M. Hopkinson, I. Vurgaftman, and J. R. Meyer, "Phase-matched second harmonic generation in asymmetric double quantum wells," Appl. Phys. Lett., 72(21), 2654-2656 (1998).
[13] J. Lee, M. Tymchenko, C. Argyropoulos, P. Y. Chen, F. Lu, F. Demmerle, G. Boehm, M. C. Amann, A. Alù, and M. A. Belkin, "Giant nonlinear response from plasmonic metasurfaces coupled to intersubband transitions," Nature, 511(7507), 65-69 (2014).
[14] J. Lee, N. Nookala, J. S. Gomez-Diaz, M. Tymchenko, F. Demmerle, G. Boehm, M. C. Amann, A. Alù, and M. A. Belkin, "Ultrathin Second-Harmonic Metasurfaces with Record-High Nonlinear Optical Response," Adv. Opt. Mater., 4(5), 664-670 (2016).
[15] C. Gmachl, A. Belyanin, D. L. Sivco, M. L. Peabody, N. Owschimikow, A. M. Sergent, F. Capasso, and A. Y. Cho, "Optimized second-harmonic generation in quantum cascade lasers," IEEE J. Quantum Electron., 39(11), 1345-1355 (2003).
[16] J. Frigerio, A. Ballabio, M. Ortolani, M. Virgilio, "Modeling of second harmonic generation in hole-doped silicon-germanium quantum wells for mid-infrared sensing," Opt. Express, 26(24), 31861-31872, (2018).
[17] J. Frigerio, C. Ciano, J. Kuttruff, A. Mancini, A. Ballabio, D. Chrastina, V. Falcone, M. De Seta, L. Baldassarre, J. Allerbeck, D. Brida, L. Zeng, E. Olsson, M. Virgilio, M. Ortolani, "Second Harmonic Generation in Germanium Quantum Wells for Nonlinear Silicon Photonics," *ACS Photonics*, **8** (12), 3573-3582, (2021).
[18] R. A. Soref, "Enabling 2 μm communications," Nature Photon., vol. 9, n. 6, pp. 1-2, June 2015.
[19] P. Vogl, H. P. Hjalmarson, and J. D. Dow, "A semi-empirical Tight Binding Theory of the Electronic Srtucture of Semiconductor," J. Phys. Chem. Solids, 44, 365, (1983).
[20] R. Saive, H. Emmer, C. T. Chen, C. Zhang, C. Honsberg, H. Atwater," Study of Interface in GaP/Si Heterojunction Solar Cell," IEEE J. Photovoltaics,8(6), 1568-1576, (2018).
[21] H. Xie, W. I. Wang, J. R. Meyer, and L. R. Ram-Mohan, "Normal incidence second-harmonic generation in L-valley AlSb/GaSb/Ga1-x

Alx Sb/AlSb stepped quantum wells," Appl. Phys. Lett., 65, 2048-2050, (1994).
[22] Y. R. Shen, "The Principles of Nonlinear Optics," Ed. Wiley, New York, (1984).
[23] G. P. Agrawal, "Nonlinear Fiber Optics," (Academic III Ed., 2001).
[24] I. Vurgaftman, J. R. Meyer, L. Ramdas Ram-Mohan, "Optimized Second-Harmonic Generation in Asymmetric Double Quantum Wells," IEEE J. Quantum Electron., 32(8), 1334-1346 (1996).
[25] C. Xiao, J. Guo, P. Zhang, C. Chen, L. Chen, L. Qian, "Effect of crystal plane orientation on tribochemical removal of monocrystalline silicon," Scientific Reports,7:40750, DOI: 10.1038/srep40750, (2017).
[26] Y. H. Zhang, D. J. Smith, "Heterovalent semiconductor structures and devices grown by molecular beam epitaxy," *J. Vac. Sci. Technol*. **A 39**, 030803 (2021).
[27] S. Sederberg, J. Firby, Y. Elezzabi, "Efficient, broadband third-harmonic generation in silicon nanophotonic waveguides spectrally shaped by nonlinear propagation," Opt. Express, 27(4), 4990-5004 (2019).
[28] J. S. Levy, M. A. Foster, A. L. Gaeta, M. Lipson," Harmonic generation in silicon nitride ring resonators,"Opt. Express, (19), 11415-11421 (2011).
[29] C. Xiong, et al. Integrated GaN photonic circuits on silicon (100) for second harmonic generation," Opt. Express, 19, 10462-10470, (2011).
[30] Z. Wang S. Ye, H. Wang, J. He, Q. Huang, S. Chang, " Machine learning method for tight-binding Hamiltonian parameterization from ab-initio band structure," *npj Computational Materials* 7:11 (2021).